Available online at www.sciencedirect.com
ScienceDirect
Coastal Engineering 53 (2006) 915–927
Coastal Engineering
An International Journal for Coastal, Harbour and Offshore Engineers
www.elsevier.com/locate/coastaleng

Parameterization and simulation of near bed orbital velocities under irregular waves in shallow water

Berry Elfrink [a,*], Daniel M. Hanes [b,1], B.G. Ruessink [c,2]

[a] Coastal and Estuarine Department, DHI Water & Environment, Agern Allé 5, DK-2970 Hørsholm, Denmark
[b] USGS Pacific Science Center, 400 Natural Bridges Drive, Santa Cruz, CA 95060, USA
[c] Department of Physical Geography, Faculty of Geosciences, IMAU, Utrecht University, P.O. Box 80.115, 3508 TC Utrecht, Netherlands

Received 4 August 2005; received in revised form 29 May 2006; accepted 1 June 2006
Available online 2 August 2006

Abstract

A set of empirical formulations is derived that describe important wave properties in shallow water as functions of commonly used parameters such as wave height, wave period, local water depth and local bed slope. These wave properties include time varying near-bed orbital velocities and statistical properties such as the distribution of wave height and wave period. Empirical expressions of characteristic wave parameters are derived on the basis of extensive analysis of field data using recently developed evolutionary algorithms. The field data covered a wide range of wave conditions, though there were few conditions with wave periods greater than 15 s. Comparison with field measurements showed good agreement both on a time scale of a single wave period as well as time averaged velocity moments.

Keywords: Wave orbital velocity; Wave height distribution; Wave skewness; Sediment transport

1. Introduction and background

The orbital water motion induced near the seabed by surface gravity waves plays an important role in the nearshore transport of sediment. Cornish (1898) was the first to relate the transport of sediment to the characteristics of a wave, in particular its shape. Cornish noticed that the onshore velocity associated with the passage of a wave crest was more effective at moving coarse sediment than the offshore velocity associated with a wave trough. In shallow water, the theory of Stokes (1847) predicts an onshore velocity associated with a wave crest that is stronger and of shorter duration than the offshore velocity associated with a wave trough. This horizontal asymmetry of the cross-shore flow, which is direct reflection of the shape of the wave, is commonly referred to as (velocity) skewness.

Inman and Bagnold (1963) were the first to formalize the importance of a skewed (horizontal oscillatory) velocity for the equilibrium of cross-shore beach slope. One of the earliest theoretical applications of Bagnold's model for bedload transport (Bagnold, 1963, 1966) was by Wells (1967), who used a finite number of Stokes waves to model the spatial variation of velocity skewness of a shoaling wavetrain. Bowen (1980) and Bailard and Inman (1981) developed Bagnold's model such that it includes moments of the velocity field, including skewness. Due to the non-linear relation between flow velocities and sediment transport, skewed waves generally cause onshore-directed sediment transport. Elfrink et al. (1999) and Doering et al. (2000) analyzed the importance of velocity skewness on cross-shore sediment transport. Under breaking waves, the mass flow in the surface roller gives rise to the generation of the so-called undertow, which contributes to the offshore transport of sediment in the surf zone. The net cross-shore transport is the result of a delicate balance between these and other onshore- and offshore-directed components. An accurate description of these components is of crucial importance for morphodynamic models that aim to simulate the evolution of cross-shore beach profiles.

* Corresponding author. Tel. +45 4516 9225.
E-mail addresses: bre@dhi.dk (B. Elfrink), dhanes@usgs.gov (D.M. Hanes), g.ruessink@geo.uu.nl (B.G. Ruessink).
[1] Tel.: +1 427 4718.
[2] Tel.: +31 30 253 2405.

0378-3839/$ - see front matter © 2006 Elsevier B.V. All rights reserved.
doi:10.1016/j.coastaleng.2006.06.002

During recent years several advanced mathematical models based on higher order Boussinesq equations have been developed; e.g. Elgar and Guza (1986), Elgar et al. (1990), Madsen et al. (1997), Veeramony and Svendsen (2000), and Kennedy et al. (2000). These models have shown reasonable agreement with measured data both in terms of time-varying orbital velocities and velocity skewness. However, advanced wave models are computationally demanding and may therefore not be appropriate for many practical coastal engineering applications. Classical wave theories such as Stokes or Cnoidal wave theory do not have a practical importance in the nearshore zone as they are not valid for irregular, breaking waves on a sloping bed. Several semi-empirical wave theories have been developed that partly overcome the shortcomings of classical wave theories (Hamm, 1996). Swart and Loubster (1978) developed a semi-empirical wave theory (vocoidal waves) for non-breaking waves on a horizontal bed. Isobe and Horikawa (1982) developed a semi-empirical model that included the effect of the bed slope. This model showed good agreement with laboratory measurements under regular waves. Grasmeijer and Van Rijn (1998) adjusted the Isobe and Horikawa (1982) model to compute onshore and offshore orbital motion under irregular waves and, in addition, modified the effect of the bed slope.

The objective of the present work is to derive a set of empirical formulations that describe important wave properties in shallow water as functions of commonly used parameters such as water depth, wave height, wave period and the local bed slope. These wave properties include phase-averaged properties such as the distribution of wave height and wave period as well as phase resolving near bed orbital velocities. In this work the term "near bed" signifies a vertical position close to the seabed but outside the wave boundary layer, which typically has a maximal thickness of a few centimeters. The empirical relations were derived on the basis of extensive analysis of field data that cover a wide range of hydrodynamic conditions. The equations are valid for irregular, breaking, and non-breaking waves on a sloped bed.

The developed set of equations is not intended to replace detailed wave modeling using advanced mathematical models, but merely as a shortcut in practical engineering applications, where advanced wave modeling studies may not be appropriate.

2. Field measurements

To analyze a broad range of hydrodynamic conditions, a large number of field data were requested and kindly made available by several colleagues. In this section the cross-shore locations of data are presented for the sites that covered the bulk of the available data. The cross-shore profiles and sampling locations are shown in Fig. 1.

2.1. Terschelling — The Netherlands

As part of the EU-funded NOURTEC project, near-bed velocity and pressure were recorded at a rate of 2 Hz at four cross-shore locations at Terschelling, Netherlands, during three six-week campaigns (Ruessink et al., 1998). The velocity measurements, which were obtained with bi-directional electro-magnetic current meters, and pressure measurements were collected in 3 to 9-m water depth, both within and seaward of the surf zone. During each experiment, morphological changes were minor. Offshore (i.e., 15-m depth) significant wave heights varied between 0.5 and 5.0 m.

2.2. Sandy Duck — North Carolina, USA

The Sandyduck97 (Hanes et al., 1998) experiments were conducted at the U.S. Army Corps of Engineers Field Research Facility in Duck, North Carolina, U.S.A. The experiment took place from September 11 to November 10, 1997. The significant wave height at the observation site in approximately 4 m water depth was typically 1 m, with a maximum of 2.7 m. Duck is a barrier island beach with medium sized sand. The data included here were collected at rates equal or greater than 2 Hz using acoustic Doppler velocimeters. The cross-shore profile in the vicinity of these measurements was fairly stable in the Sandyduck97 experiment. Experiment details and observations can be found in Hanes et al. (2001).

2.3. Egmond aan Zee, The Netherlands

In the framework of the EU sponsored Coast3D project, near-bed velocity and pressure were recorded at a rate of 2 Hz at four

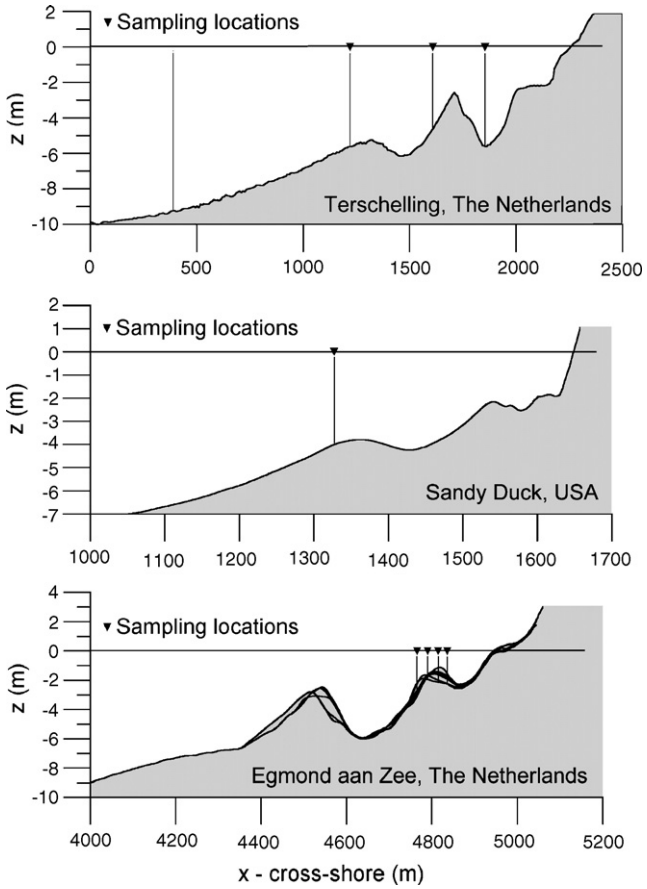

Fig. 1. Cross-shore profiles and sample locations at Terschelling(top), Sandy Duck(middle) and Egmond (bottom).

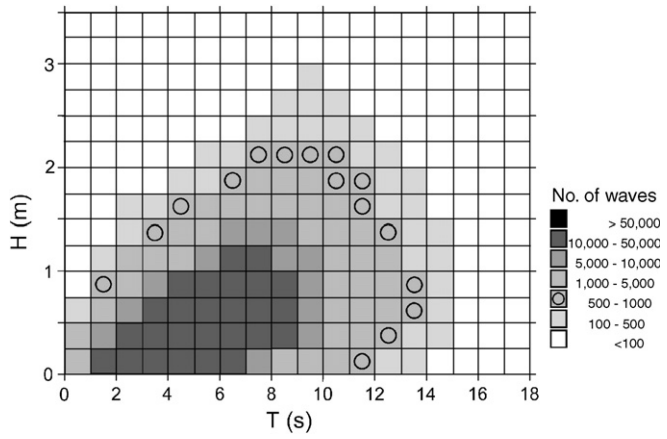

Fig. 2. Data coverage in terms of wave height H and wave period T.

positions across the inner subtidal bar at Egmond aan Zee, The Netherlands during October and November 1998 (Ruessink et al., 2001). Equipment similar to the NOURTEC project was used. The data were collected in 1 to 4 m water depth, and offshore significant wave heights reached values up to 5.5 m. During the experiment, considerable changes in the cross-shore morphology were observed, consisting both of cross shore bar migration and alongshore non-uniform variability (Ruessink et al., 2000). The variations in the cross-shore profile are indicated as envelopes (solid lines in the plots). As a consequence of these profile changes, sensor heights off the bed varied considerably. This had led to some problems in determining the exact positions of the equipment, which in some cases was buried during the experiment.

3. Data analysis

All velocity data were band-pass filtered with cutoff frequencies of 0.05 and 1 Hz in order to remove fluctuations that were not directly related to the orbital motion of the waves. Analysis has shown that the energy related to frequencies above 1 Hz generally was very low and is neglected in this analysis. To calculate the orbital velocity in the direction of wave propagation, the cross-shore and longshore velocity components were projected into the mean wave direction, which was estimated from the time averaged flow velocities:

$$\alpha = \frac{\overline{u_x u_y}}{\left|\overline{u_x u_y}\right|} \tan^{-1}\left(\left|\frac{\overline{u_y}}{\overline{u_x}}\right|\right) \quad (1)$$

Here α is the angle between the wave incidence and shore normal; u_x and u_y are the cross-shore and longshore velocity components, respectively. The horizontal bar indicates time-averaged quantities and the vertical bars indicate absolute values. Obviously this is not a very accurate method to determine the wave direction. However, as most of the measurements were obtained in shallow water, the angles of wave incidence were small, and possible errors in the wave angle had only a very small effect on the resulting velocities in the wave direction. The water level fluctuations were derived through linear transfer of the pressure signal. The height of each individual wave was calculated as the difference between maximal and minimal water level elevation observed during one individual wave period, defined as the time interval between two successive zero up crossings.

The field data used in this analysis covered a range of wave conditions. Fig. 2 shows the observed number of individual waves for a number of discrete classes of wave period T and wave height H. It should be noted that the data range only include a limited number (<100) of storm wave heights above about 3 m and periods greater than 15 s typical of Pacific and Antarctic ocean storms.

Fig. 3 shows the data coverage in terms of the normalized wave height $H^* = H/h$ and the normalized wave length $L^* = L/h$ where H is the height of an individual wave, h is the local water depth, and L is the wave length calculated according to Airy wave theory: $L = L_o \tanh(kh)$, $L_o = (g/2\pi)T^2$, T=wave period of the individual wave. The water depth h was calculated as the average value of the total water depth during each burst, which had a typical duration of 20 min.

The data coverage in terms of the surf similarity parameter or Irribarren number, ξ, is shown in Fig. 4. The value of ξ is defined here as:

$$\xi = \frac{\tan\beta}{\sqrt{(H/L_o)}} \quad (2)$$

Here, β is the local bed slope. The value of β is defined here as the mean slope measured over a distance of twice the local wavelength seaward of the sampling location. The bed slope is defined as positive if the slope is upward toward the shoreline.

4. Characteristic velocity parameters

The time varying orbital near-bed velocity for each individual wave in a wave train is assumed determined by a few characteristic velocity parameters. These parameters are the maximum velocities under wave crest, and trough, their respective phases and the phase of the zero down crossing, as shown in Fig. 5.

For monochromatic waves in constant water depth these parameters can be derived from classical wave theories. However, for individual waves in wave groups propagating over a sloping bed no easy theoretical solutions exist. Therefore, empirical expressions were derived on the basis of the available wave measurements. Analogous to classical wave theories, expressions for characteristic velocity parameters are derived as functions of H^*, L^* and ξ.

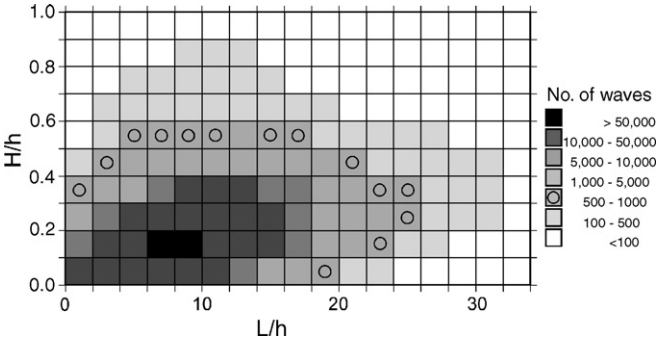

Fig. 3. Data coverage in terms of H/h and L/h.

The major part of the field data was sampled with a frequency 2 Hz. Periods of individual waves were typically between 4 s and 9 s. With only a few observations per wave period the time varying orbital velocity and surface elevation for individual waves cannot be resolved very well. In particular the extreme values, that is, the orbital velocities under the wave crest and the wave trough, cannot be resolved well; see Tayfun (1993) and Hamm and Peronnard (1997) for a detailed analysis. Instead of using the signals of the individual waves directly, ensemble averaged values of the time varying orbital velocity were calculated. First, a discrete number of equidistant intervals was determined covering the entire range of observed H^*, L^* and ξ values. Approximately 20 equidistant intervals were selected for the three independent variables. Theoretically this leads to $20\times20\times20$ combinations of H^*, L^* and ξ. However, many combinations are not present or only have a few members in the data set. Intervals with less than 500 data records were disregarded in the analysis. For each identified interval the ensemble-averaged intra-wave velocity variation was calculated. A time resolution of 40 time steps per period was used. By using a large amount of data, random fluctuations are filtered out.

The time resolution of 40 time steps per period used in the ensemble-averaging procedure gives a better description of the time varying orbital velocity than the raw data signals. However, if the peak velocities were derived directly from ensemble averaged values, then a slight underestimation of these peak values would be introduced. In order to alleviate this problem, the ensemble averaged velocity variations in each class were approximated by higher-order Forsythe polynomials (Forsythe, 1957). From these polynomial fits the following 5 characteristic velocity parameters were derived, see definition sketch in Fig. 5:

$$U_1 = U_C/(U_C + U_T) \tag{3}$$

$$U_2 = {}_{1/2}(U_C + U_T)/\hat{U}_{Airy} \tag{4}$$

$$T_1 = T_C/T \tag{5}$$

$$T_0 = T_Z/T \tag{6}$$

$$T_2 = T_T/T \tag{7}$$

U_1 is a measure of skewness, where a value of 0.5 corresponds to a sinusoidal wave and a value of 1 to a solitary wave. U_2 is the ratio of the velocity amplitude and the velocity amplitude for Airy waves, $\hat{U}_{Airy}$. The variables T_1, T_0 and T_2 are the phases of the maximal velocity under the wave crest, the zero down crossing, and the maximal velocity under the wave trough, respectively.

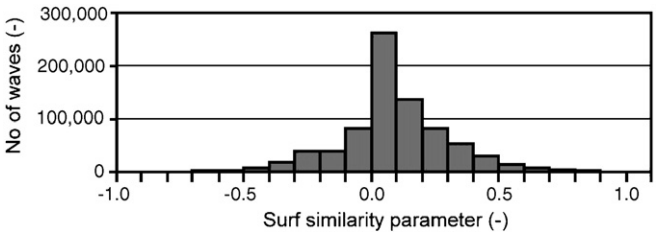

Fig. 4. Data coverage in terms of the surf similarity parameter ξ.

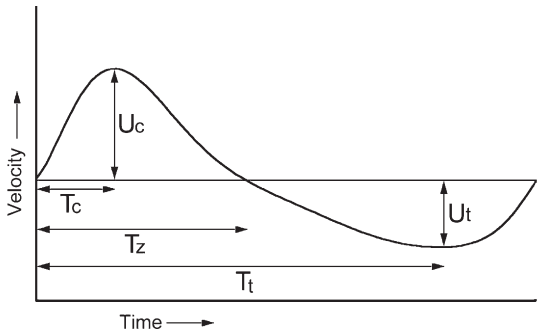

Fig. 5. Definition sketch of normalized near bed orbital velocities.

Empirical expressions were derived to relate the velocity parameters (Eqs. (3)–(7)) to the wave parameters H^*, L^*, and ξ. The expressions were derived using recently developed data mining techniques (evolutionary algorithms) as developed by Keijzer and Babovic (1999). The basic principle of this technique is that an initial population of formulae is generated randomly from the input data. The performance of each formula is evaluated on the basis of a number of predefined criteria. In our case two criteria were chosen: (1) the correlation between predicted and observed data and (2) the size of the formula. On the basis of the evaluation a number of "parents" were selected, typically a value of 200 was used. By randomly combining substructures of the parents a new generation (equal to the population of formulae) is created. Substructures are replaced by randomly generated new substructures (mutations). The newly derived population is evaluated and the process is repeated. Optimal formulae are usually derived after approximately 20 to 50 generations.

The output of the evolutionary algorithm is a large number of formulae with different performance on the selected criteria. Usually the formulae with the highest correlations are complex and long. Formulae with high scores on the second criterion (size of the formula) have lower correlations. The choice of the optimal formula is a matter of "taste." As all formulae are easily programmable in any program code, the highest priority was given here on the correlation, rather than the size of the formula. A disadvantage of this is that the formula becomes rather inscrutable; it may become impossible to observe or infer clear physical meaning from the expression.

The data were not uniformly distributed over the entire range of dependent variables. In order to equalize the weight of common and rare events, a statistical analysis was performed on the raw data set. Then averaged values of the dependent variables were calculated for the identified intervals in H^*, L^*, ξ space as mentioned in Section 4.

Expressions for the velocity parameters are given in Appendix A. Fig. 6 shows the comparison between measured values of the 5 characteristic velocity parameters and the values predicted using the derived analytical expressions. The correlation factor r^2 is indicated in each graph. The figures show that the agreement is satisfactory despite some scatter.

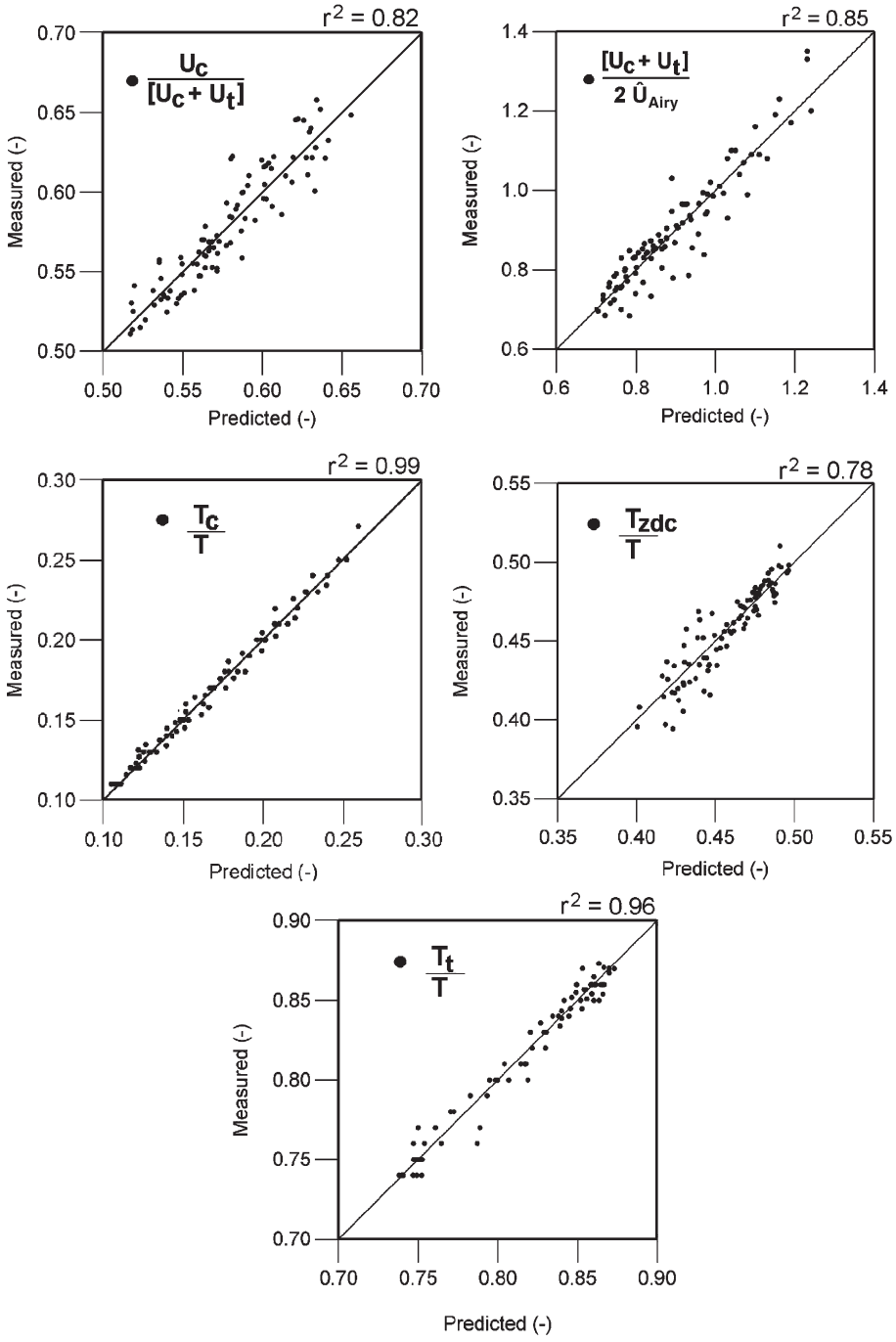

Fig. 6. Comparison predicted and measured velocity parameters.

Direct comparison with existing wave theories is not appropriate because such wave theories are not valid for irregular, breaking waves on a sloping bed. However, in many engineering applications Airy wave theory is applied, even in areas beyond its validity. Therefore, some comparison of the present model with Airy wave theory seems justified. Fig. 7 (top) illustrates the calculated variation of U_1 with H^* and L^* for a constant bed slope of 1:20. The shaded area covers the area that is not or only sparsely covered by the field data. A value of $U_1=0.5$ thus corresponds to an equal magnitude of the maximal velocity under the wave crest and under the wave trough, as is the case for Airy wave theory. A higher value indicates higher velocities under the crest than under the trough. It was found that the strongest asymmetry occurs for $L^* \approx 10$. For higher values of L^* the asymmetry decreases and the velocities under wave crest and trough become equal for $L^* \approx 30$. The asymmetry was found to increase with H^*. The increase of the asymmetry with the Ursell number Us, defined here as $Us=HL^2/h^3$, for small values of H^* and L^* is consistent with higher order wave theory for a horizontal bed.

Fig. 7 (bottom) shows the variation of U_2 for the same conditions as above. A value of 1 corresponds to the orbital velocity amplitude that is equal to the amplitude calculated from

Airy wave theory. It was found that for low values of H^* and L^*, the velocity amplitude is very similar to Airy wave theory. For increasing H^* and L^* it was found to decrease.

Another interesting feature of the derived expressions is the importance of the bed slope on the ratio of the maximum velocities under crest and trough. The ratio between crest and trough velocities is very important for cross-shore sediment transport and the associated equilibrium bed slope and profile shape for given hydrodynamic conditions. Fig. 8 shows the calculated difference between crest and trough velocity along the L^* axis for varying bed slopes. The wave height H^* was kept constant at 0.5. It was found that $(U_C - U_T)$ increases independent of the bed slope until it reaches a maximum for L^* around 10. The Ursell number, *Ur*, is indicated on top of the figure. For $L^* > 10$, $(U_C - U_T)$ decreases with L^* and with bed slope. For steep slopes the derived expressions even suggest negative values, thus indicating larger velocities under the trough than under the crest. It is noted however that insufficient number of wave records were available for $L/H > 25$ and a bed slope of 1 : 15 to confirm this. The dashed parts of the curves in Fig. 8 represent values that are beyond the range of the field data and can therefore not be confirmed. The expressions of the velocity parameters are entirely empirical. Therefore, application of the expressions in the range not covered by the field data may lead to erroneous results and is not recommended.

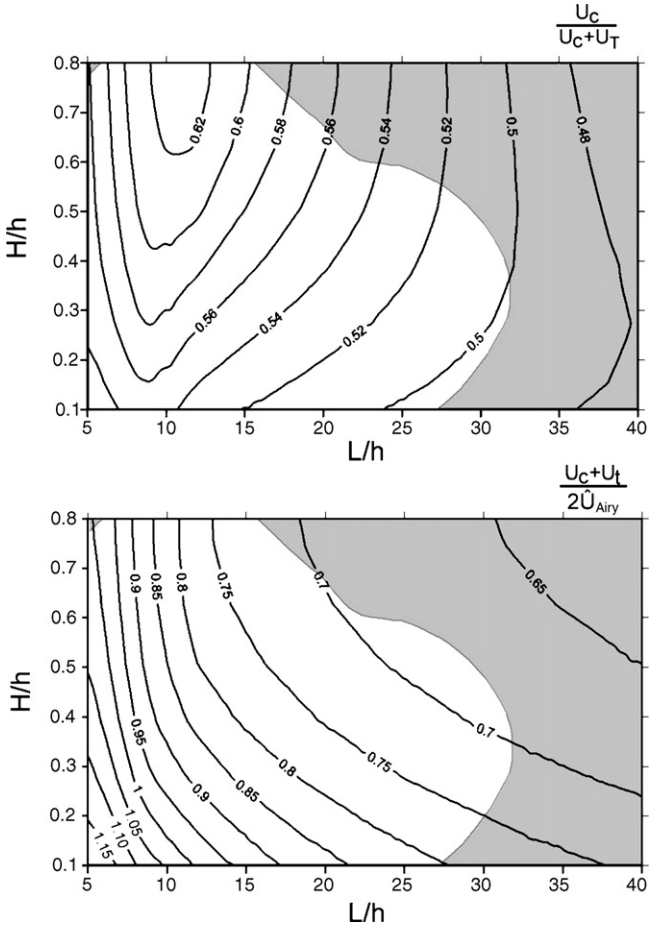

Fig. 7. Calculated variation of velocity parameters. Top: normalized maximal velocity under the wave crest, Bottom: normalized orbital velocity range. Bed slope = 1:20.

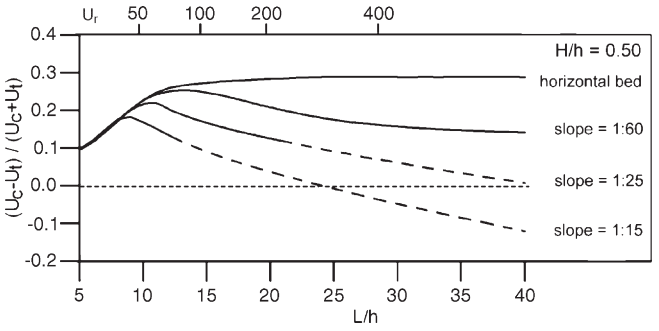

Fig. 8. Difference between max velocities under wave crest an trough for various bed slopes.

5. Time variation of orbital velocity

To derive a continuous time varying orbital velocity from the 5 velocity parameters a certain shape must be assumed between maximal velocities and the zero crossings. A number of shapes were tested and the best results were obtained using a set of simple sinusoidal functions for each segment between the maximum velocities and the zero crossings. This approach is similar to the method originally proposed by Isobe and Horikawa (1982). In order to fulfill the requirement of zero mean velocity, a correction term must be included. Several procedures were tested. The data analysis showed that the shape of the velocity distribution between the wave crest and zero down crossing was usually concave and not convex as predicted by a sine function. By superposing an additional sine function between the wave crest and zero down crossing, the shape of the orbital velocity was best captured, while maintaining zero mean velocity. The amplitude of this additional velocity, U_0, is found from the derived velocity parameters.

The expressions for time varying orbital velocity read:

$$U(t) = U_C \sin[1/2\,\pi t/T_1] \qquad 0 < t < T_1 \tag{8}$$

$$U(t) = U_C \cos[1/2\,\pi(t-T_1)/(T_0-T_1)] - U_0 \sin[\pi(t-T_1)/T_0-T_1] \qquad T_1 < t < T_0 \tag{9}$$

$$U(t) = -U_T \sin[1/2\,\pi(t-T_0)/(T_2-T_0)] \qquad T_0 < t < T_2 \tag{10}$$

$$U(t) = -U_T \cos[1/2\,\pi(t-T_2)/(1-T_2)] \qquad T_2 < t < 1 \tag{11}$$

Where $t = \dfrac{t'}{T}$ and t′ = time (s)

The velocity amplitudes U_C, U_T and U_0 are calculated as:

$$U_C = U_1 U^* \tag{12}$$

$$U_T = U^* - U_C \tag{13}$$

$$U_0 = [U_C T_0 - U_T(1-T_0)]/(T_0-T_1) \tag{14}$$

where $U^* = 2U_2\hat{U}_{Airy}$

Fig. 9 shows examples of the shape of time varying orbital velocities calculated from Eqs. (8)–(14) for a number of intervals in the H^*, L^*, ξ domain. Fig. 9 (top) shows the time varying orbital velocity for 3 waves with different wave lengths in a constant water depth of 2 m. The value of H/h was kept constant at 0.4 in all cases and the bed slope was 1:40. It was found that the velocity variation becomes increasingly asymmetric for increasing L/h. The maximal velocities under the wave crest occur for $L/h=10$. Both for $L/h=5$ and $L/h=25$ the crest velocities are lower. The maximal velocities under the wave trough are considerably less affected by L/h than the velocities under the crest.

Fig. 9 (center) shows the orbital velocities for varying H/h. The value of L/h was constant at 15, the water depth was 2 m and the slope was 1:40. The phase of the maximal velocity is seen to be nearly constant for all 3 wave heights. The velocity maxima both under wave crest and trough increase with increasing H/h.

Fig. 9 (bottom) shows the orbital velocities for varying bed slope. The values of L/h and H/h were 15 and 0.5 respectively. The water depth was 2 m. The bed slope does not affect the phase of the maximal flow velocities under wave crest and trough. However, an increase in bed slope will reduce the maximal velocities in the wave direction and increase the maximal velocity opposite to the wave direction. This is an interesting phenomenon that may be important for cross shore sediment transport and the beach profile.

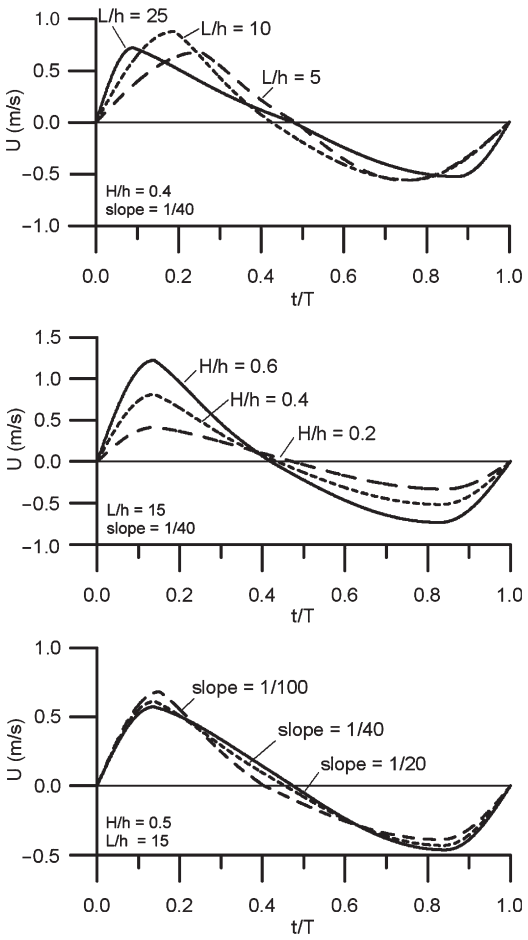

Fig. 9. Examples of calculated time varying orbital velocities for varying wave length (top), wave height (center) and bed slope (bottom).

6. Direct comparison with measured time varying orbital velocities

To evaluate the ability of the derived expressions to reproduce characteristic time series of orbital velocities under natural wave groups, a comparison was made with measured data.

First a measured record of water level variations was transformed to an array of individual waves. The period of these individual waves was determined by two successive down crossings, the wave height was taken as the difference between maximal and minimal surface elevation. For each individual wave period the time varying orbital velocities were calculated using the newly derived expressions. The derived synthetic time series of orbital velocities was compared with measured velocities. Fig. 10 shows examples for a number of situations. Even though the same data was included in the derivation of the expressions for orbital velocities, the effect of one single data record on these expressions is very small due to the large amount of data used in the derivations. Therefore, comparison with measured data, although not a formal model validation, is justified to illustrate the behavior of the present model.

Even though variations occur, the agreement between measured and simulated velocities is satisfactory. It is noted that the measured data may contain velocity fluctuations on time scales that are different from the principal wave period. These fluctuations cannot be resolved by the above expressions.

7. Time averaged properties: U_{rms} and skewness

In many coastal engineering applications wave conditions are represented by time averaged properties. For the calculation of sediment transport, time-averaged properties such as U_{rms} and velocity skewness are important and a comparison was made between simulated and measured values. The simulated values were calculated on the basis of the above procedure of replacing individual waves in wave groups by synthetically generated near-bed orbital velocities.

The value of U_{rms} of the measured data was calculated directly from the filtered time series of orbital velocities. The duration of each time series (e.g. burst) was 20 min. In some cases the duration was 40 min. Fig. 11 shows the measured and simulated U_{rms} for all wave data. Even though some scatter is observed, the general agreement is good. The model was found to slightly under-predict the measured U_{rms}. This is expected due to the fact that oscillations with frequencies higher than the wave period defined by two successive down-crossings contribute to the measured U_{rms}, but are not resolved in the synthetically generated time series.

Doering and Bowen (1995) and Doering et al. (2000) developed empirical expressions for velocity skewness under natural waves. The present equations for orbital velocities were

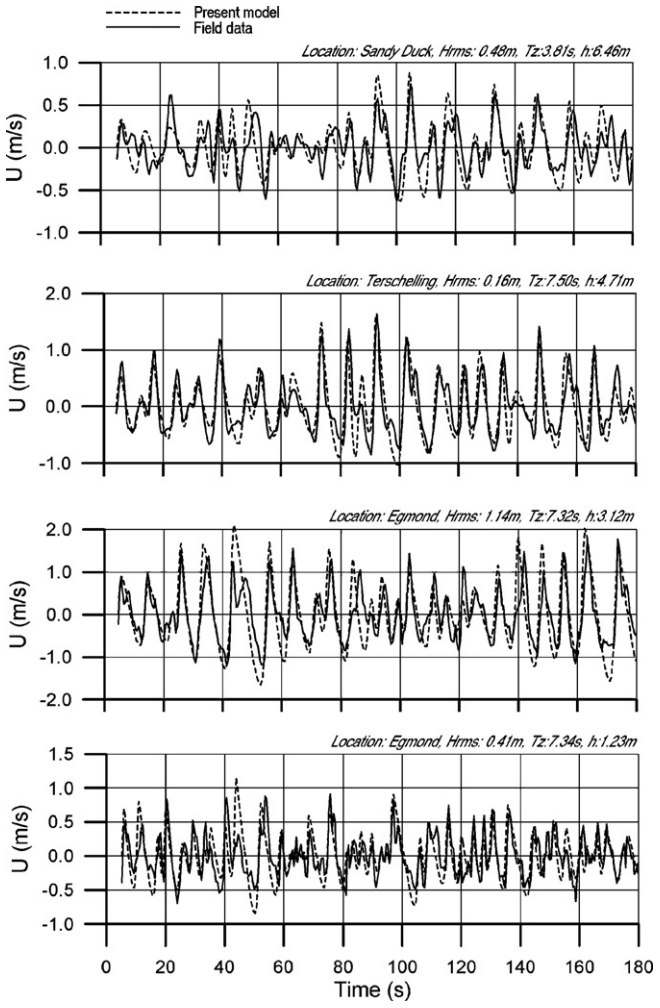

Fig. 10. Comparison between present model and field data.

not derived explicitly to resolve skewness. However, velocity skewness, S, can be easily be derived from the expressions as:

$$S = \frac{\overline{U^3}}{U_{\mathrm{rms}}^3} \tag{15}$$

Fig. 12 shows the comparison between simulated and measured skewness. The scatter is higher than for U_{rms}. This is not surprising as the expressions were not derived with skewness as a dependent parameter. The resulting skewness is thus affected by the assumptions made to calculate the continuous time variation of the orbital velocities. Another reason for the observed scatter is the fact that velocity skewness is not entirely determined by local conditions. The history of the wave is an important and sometimes perhaps even dominating factor that is not included in the present model. Even though the variation is considerable some agreement was found between the mean values and the measured data.

8. Wave height distribution

In order to derive synthetic time series from statistical wave parameters such as H_{rms} and T_z, the joint wave height-period distribution must be known. Klopman (1996) used a modified Glukhovskiy distribution, which is a special case of the more general Weibull distribution. He found an empirical expression for the shape parameter m (see Eq. (17) below) that was able to reproduce laboratory data well:

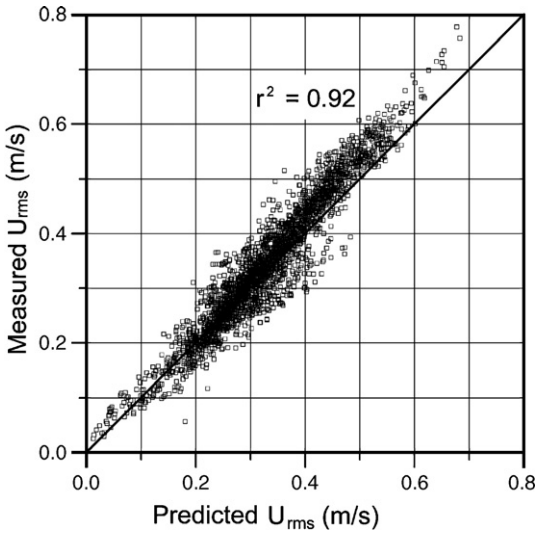

Fig. 11. Predicted and measured U_{rms}.

$$m = \frac{2}{1 - 0.7H_{\mathrm{rms}}/h} \tag{16}$$

Battjes and Groenendijk (2000) proposed a composite Weibull distribution and obtained good results for wave flume data. They used a shape factor of $m=2$ for the lower waves (Rayleigh distribution) and a value of $m=3.6$ for the higher waves. In the present analysis an expression similar to Klopman (1996) was sought, but based on field data rather than laboratory data. An analysis was performed upon the available data set. Similar to the derived formulae for the orbital velocities under individual waves, analytical expressions were sought to resolve the wave height-period distribution as functions of H_{rms}, T_z and water depth.

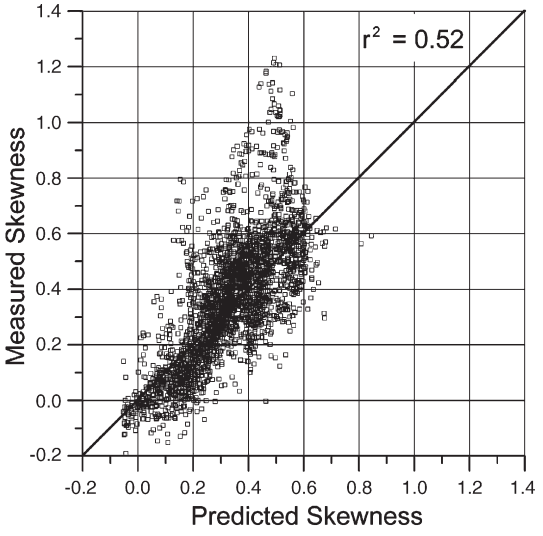

Fig. 12. Predicted and measured skewness.

Similar to Klopman (1996) the wave heights were assumed to follow the general Weibull distribution:

$$p(H) = \frac{mA}{H_{\mathrm{rms}}}\left(\frac{H}{H_{\mathrm{rms}}}\right)^{m-1} \exp\left\{-A\left(\frac{H}{H_{\mathrm{rms}}}\right)^{m}\right\} \quad (17)$$

With $A=[\Gamma(x)]^{m/2}$ and $x = 1+\frac{2}{m}$, and Γ is the gamma function.

The shape of the wave height distribution as function of m is illustrated in Fig. 13 (left). A value of $m=2$ corresponds to the Rayleigh distribution. Similar to the parameterization of the orbital velocity parameters, the evolutionary algorithm was used to find an analytic expression for the exponent m. The analysis has shown that m mainly varies with the ratio of the root mean square wave height, H_{rms}, and the water depth h:

$$m = 15.5\left[\tanh\left(\frac{H_{\mathrm{rms}}}{h}\right) - \left(\frac{H_{\mathrm{rms}}}{h}\right)^{2}\right]^{2} + 2.03 \quad (18)$$

Good agreement was found between measured and simulated values of m as shown in Fig. 13 (right). It is noted that the dots indicate the average value of measured m for a specific class in the H^*–L^*–ξ space, similar to the analyses for the wave velocity parameters.

Fig. 14 shows the comparison between measured and predicted data for the expression of Klopman (1996) and the present model (e.g. Eq. (18)). The two expressions were found to give quite similar results for relative low wave heights. For $H_{\mathrm{rms}}/h>0.4$ the present analysis shows a decreasing value of m whereas Klopman (1996) predicts an increasing value. However, there are too few data points to evaluate the proper shape of the curve at large wave height to depth ratios.

9. Wave height–period distribution

It was assumed that some relation exists between the period and height of the individual waves in the wave groups, and that for each wave height in the wave group a "most likely" wave period exists. The evolutionary algorithm was applied on the entire data set and an expression was found for the normalized wave period of the individual wave (T/T_z):

$$\frac{T}{T_z} = 1 + 0.042\left[\frac{H}{H_{\mathrm{rms}}} + \left(\frac{L_m}{h}\right)\left(\frac{H}{H_{\mathrm{rms}}}\left[\frac{H_{\mathrm{rms}}}{h}\right]^{0.25} - 1\right)\right] \quad (19)$$

Here, T and H are wave period and wave height for the individual wave in the wave group respectively. L_m=wave length calculated from Airy wave theory using T_z and the local water depth h.

The relation between measured and predicted T/T_z is shown in Fig. 15. The agreement was found to be good.

Fig. 16 shows the derived variation of the "most likely" wave period as a function of the wave height. The dashed curves correspond to $L^*=10$, the solid lines to $L^*=20$.

For each value of L^*, periods for three different values of H^* are shown. It is interesting to note that for the longer wave e.g. $L^*=20$, the range of wave periods varies between approximately 0.2 to 2.5 times the mean wave period whereas the periods for the shorter wave are considerable closer to the mean wave period. Furthermore it was found that the range of wave period increases with H^*.

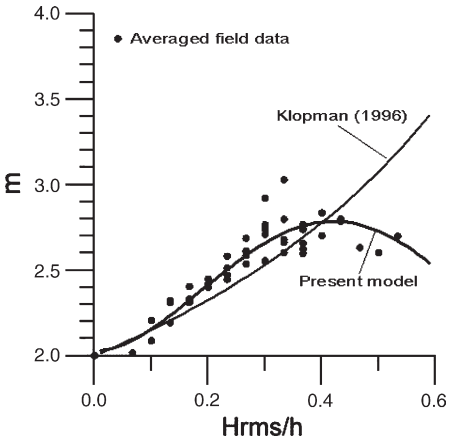

Fig. 14. Comparison between measured and predicted values for m.

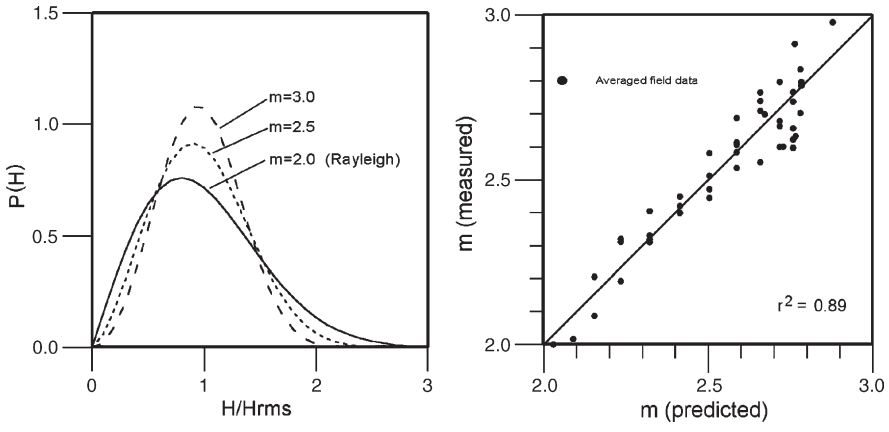

Fig. 13. Left: Illustration of wave height distribution as function of the exponent m. Right: Comparison between predicted and measured values of m.

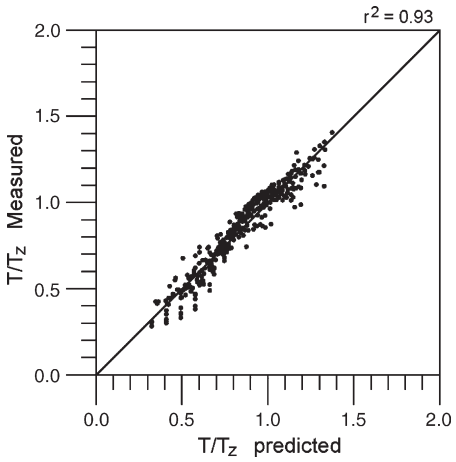

Fig. 15. Comparison between measured and predicted wave periods for individual waves in a wave group.

Obviously, each wave height in a wave group is not strictly connected to one single period, but rather a distribution of wave periods around the "most likely" period. An analysis of the variation of the wave period around the most likely period showed that the standard deviations of the measured wave periods were found to vary between $0.1T_z$ and $0.4T_z$.

10. Calculating time-averaged properties from common wave parameters

Previously, the time-averaged properties were calculated by replacing each individual wave in the wave record by a synthetically generated wave (see Figs. 11 and 12). Now we go one step further and calculate U_{rms} and skewness using a synthetically generated wave train, calculated from the derived expressions for wave height distribution and wave height–period relations. From measured H_{rms}, T_z, bed slope, and water depth the wave height distribution was calculated using Eqs. (16) and (17). From this distribution a number of 50 wave heights with equal probability were derived. For each wave a corresponding wave period was calculated using Eq. (19). Finally, Eqs. (8)–(14) were used to calculate the wave orbital velocities for each wave. The analysis was performed for all available wave records. Fig. 17 shows the

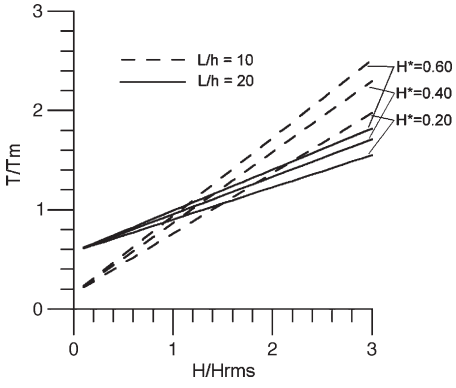

Fig. 16. Variation of wave period as function of wave height for different values of L^* and H^*.

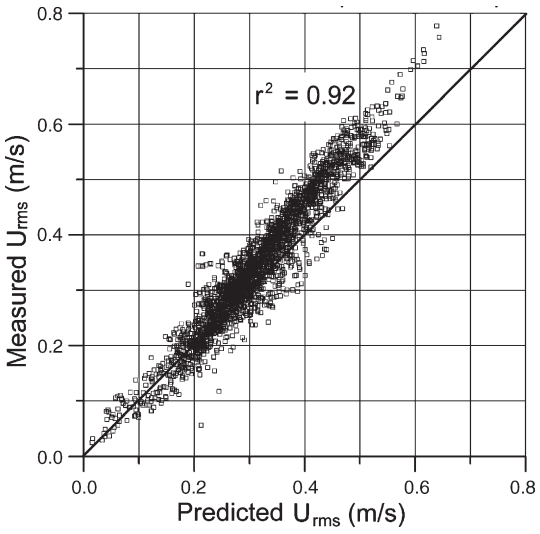

Fig. 17. Predicted and measured U_{rms}.

measured and simulated U_{rms} for all wave data. Despite the scatter the averaged values are reasonably well reproduced by the present method.

Fig. 18 shows the measured and simulated skewness. The variation is considerably larger than for U_{rms}. The scatter diagram shows a cloud of records under the line of perfect agreement in the range 0.7–0.9 of the predicted skewness. It is noted that the majority of these records originate from the innermost sampling location of the Egmond experiments as shown in Fig. 1. The measurements were performed shoreward of the crest of a bar that appeared quite dynamic during the field experiments. It is possible that the local morphology has been subject to variations that were not captured by two subsequent measurements of the cross-shore profile.

Furthermore, the site is characterized by strongly non-uniform depth contours. The effect of such complex bathymetry on the velocity skewness, and the history of the waves that propagate over it cannot be resolved well by the present model.

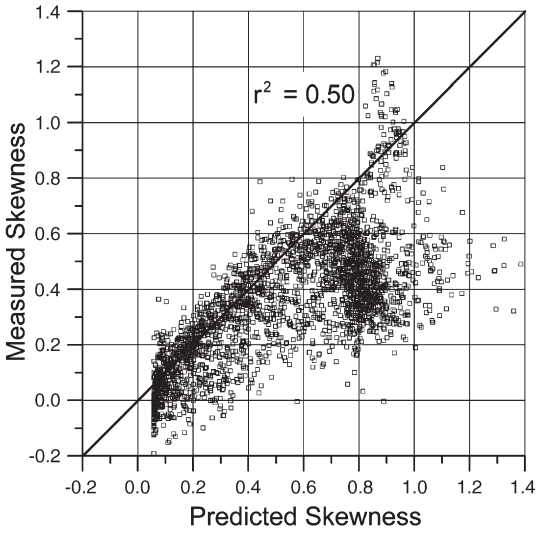

Fig. 18. Predicted and measured skewness.

The results obtained for other sampling sites show considerably better agreement between predicted and measured skewness.

11. Conclusions

On the basis of field measurements of near bed orbital velocity, a set of empirical expressions were derived for characteristic velocity parameters as functions of 3 independent dimensionless wave parameters: the normalized wave height, wave length, and the local Irribarren number. Comparison with measured data showed good agreement for both phase resolving near-bed orbital velocities and their time averaged properties such as U_{rms} and skewness.

Similar to the derived expressions for orbital velocities, expressions were derived for the distribution of wave height and wave period as functions of common wave parameters such H_{rms} and T_z and the water depth h. These expressions show good agreement with the measured data.

By combining the two sets of derived expressions, synthetic time series of near bed orbital velocities were generated from H_{rms}, $T_{z,}$, local bed slope β, and h. Comparison with measured data showed good agreement for U_{rms}. The agreement between measured and simulated velocity skewness was not as good as for U_{rms}. The poorest agreement between predicted and measured skewness was obtained for measurements originating from complex bathymetries. It is noted the expressions presented in this paper were not explicitly derived for skewness as a dependent parameter. The relative large amount of scatter is therefore not unexpected. Taken into account that velocity skewness is not entirely determined by local conditions, the agreement with field data was found quite satisfactory.

As the primary technique used to derive the results was curve fitting of empirical data, extrapolation of the results beyond the range of the empirical data it was based upon is not recommended.

12. List of symbols

α	Angle between wave incidence and shore normal (°)
β	Bed slope (–)
ξ	Surf similarity parameter or Irribarren number (–)
A	Coefficient in Weibull distribution (–)
H	Height of individual wave in wave train (s)
H^*	Normalized height of individual wave in wave train (–)
H_{rms}	Root mean square wave height (m)
h	Water depth (m)
L^*	Normalized length of individual wave in wave train (–)
L_o	Deep-water wave length calculated form linear wave theory (m)
m	Exponent in Weibull distribution (–)
S	Velocity skewness (–)
T_z	Zero down crossing wave period (s)
T_1	Normalized phase of wave crest (–)
T_0	Normalized phase of zero down crossing (–)
T_2	Normalized phase of wave trough (–)
t	Time (m/s)
T	Period of individual wave in wave train (s)
u_x	Cross-shore component of orbital velocity (m/s)
u_y	Longshore component of orbital velocity (m/s)
U	Time varying orbital velocity (m/s)
$\bar{U}$	Time averaged flow velocity (m/s)
U_{rms}	Root mean square velocity (m/s)
$\hat{U}_{Airy}$	Orbital velocity amplitude according to Airy wave theory (m/s)
U_1	Normalized maximal orbital velocity (–)
U_2	Velocity asymmetry parameter (–)
U_C	Maximal orbital velocity under wave crest (m/s)
U_T	Maximal orbital velocity under wave trough (m/s)
U_0	Amplitude of velocity correction (m/s)
U^*	Sum of orbital velocity amplitudes under wave crest and trough (m/s)
Ur	Ursell number (–)

Acknowledgments

B. Elfrink is partly supported by EPCOAST (Exploitation and Protection of Coastal Zones) which is funded by the Danish Research Agency, Ministry of Science, Technology and Innovation, STVF under contract no. 26-00-0144. D.M. Hanes was supported financially by the USGS Coastal and Marine Geology Program, the Coastal Science Program of U.S. Office of Naval Research, and the National Science Foundation through the National Ocean Partnership Program. B.G. Ruessink was supported by the Netherlands Organization for Scientific Research (NWO) under contract 864.04.007.

The authors would like to express their gratitude to the following persons for their kind assistance in providing the field data used in this study: Richard Soulsby (HR-Wallingford, UK), Agustín Sánchez-Arcilla and César Mosso Aranda (UPC, Spain), Travis Mason and Karen Stapleton (Univ. of Plymouth, UK), Gerd Masselink (Univ. of Loughborough, UK), Jon Williams and Judith Wolf (POL, UK), James Kirby (Univ. of Delaware, USA), James Kaihatu (Naval Research Laboratory, Stennis Space Center, USA), Erik Jan Houwing, (Rijkswaterstaat, The Netherlands) and Geoff Smith, (CSIR, South Africa). We wish to thank Luc Hamm, Peter Ruggiero and Jingping Xu (USGS) for their valuable comments on the manuscript.

Appendix A. Empirical expressions

General wave parameters

$$H^* = H/h$$

$$L^* = L/h$$

$$\xi = \frac{\tan\beta}{\sqrt{H/L_o}}$$

$$Ur = H^* L^{*2}$$

Orbital velocity parameters

$$U^* = 2U_2U_{\text{Airy}}$$

$$U_C = U_1U^*$$

$$U_T = U^*-U_C$$

$$U_0 = \frac{U_CT_0-U_T(1-T_0)}{T_0-T_1}$$

Correction for large values of U_0:

if $U_0 > 0.25U_C$ then

$$U_0 = 0.25U_C$$

$$a_1 = \frac{(-U_T + T_1U_0)}{T_0[U_0-U_C-U_T]}$$

if $a_1 < 0.99$ then

$$T_0 = 0.99T_0$$

$$U_T = \frac{[-(T_0-T_1)U_0 + T_0U_C]}{1-T_0}$$

if $a_1 \geq 0.99$ $T_0 = a_1T_0$

Derived expression for U_1

$$C_1 = L^*-10$$

$$C_2 = |C_1-(H^*-|\xi|)|$$

$$C_3 = \xi(1-C_1)$$

$$C_4 = \tanh(|C_3-C_2|/Ur)$$

$$C_5 = \sqrt{(|\xi| + \tanh(C_4))}$$

$$P_1 = \sqrt{H^*}-C_5H^*$$

$$a_1 = 0.38989$$

$$b_1 = 0.5366$$

$$U_1 = b_1P_1 + a_1$$

Derived expression for U_2

$$d_1 = 3\xi + 2(L^*/Ur)$$

$$d_2 = \sqrt{L^*} - \tanh(|d_1|)$$

$$d_3 = \left(2\xi + \sqrt{L^*/Ur}\right)^2$$

$$d_4 = Ur + L/(d_3Ur)$$

$$d_5 = \sqrt{d_2/d_4}$$

$$P_2 = 1.2001d_5 + 0.4758$$

$$a_2 = -0.0145$$

$$b_2 = 1.1600$$

$$U_2 = b_2P_2 + a_2$$

Derived expression for T_1

$$e_1 = H^*L^*\xi$$

$$e_2 = e_1[-9.8496\,\xi H^*]^2$$

$$e_3 = \tanh(e_2) + \tanh(e_1) + L^*-1$$

$$P_3 = \tanh(-9.3852/e_3)$$

$$a_3 = -0.0005$$

$$b_3 = -0.2615$$

$$T_1 = b_3P_3 + a_3$$

Derived expression for T_0

$$f_1 = 0.0113\xi\,L^{*2}$$

$$f_2 = 3.5667 \times 10^{-4}\,\xi L^{*4}$$

$$f_3 = 0.1206L^*\tanh(\tanh(\xi))$$

$$f_4 = H^*\tanh(f_2)/\tanh(f_3)$$

$$P_4 = H^*\tanh(0.02899L^*(f_1))-\tanh(f_4)$$

$$a_4 = 0.5028$$

$$b_4 = 0.0958$$

$$T_0 = b_4P_4 + a_4$$

Derived expression for T_2

$$g_1 = \xi + 0.9206$$

$$g_2 = L^*-\sqrt{Ur} + \sqrt{(2.5185/L^*)}-4.6505$$

$$g_3 = \sqrt{|g_2/H^*|}$$

$$g_4 = |L^* + \xi|-4.4995 + \xi$$

$$g_5 = |g_4 + |\xi|-5.3981|$$

$$g_6 = |L^* + \sqrt{3.0176/H^*}-5.2868 + H^*|$$

$$g_7 = |\xi + 0.1950(g_6 + \xi)|$$

$$g_8 = |\xi| + L^*$$

$$P_5 = \frac{4.1958}{g_1 + g_3 + g_5 + g_7 + g_8}$$

$$a_5 = 0.9209$$

$$b_5 = -0.5623$$

$$T_2 = b_5 P_5 + a_5$$

References

Bagnold, R.A., 1963. Mechanics of marine sedimentation. Sea 3, 507–528.

Bagnold, R.A., 1966. An approach to the sediment transport problem from general physics. U. S. Geol. Surv. Prof. Pap. 422-I 37 p.

Bailard, J.A., Inman, D.L., 1981. An energetics bedload model for a plane sloping beach: local transport. J. Geophys. Res. 86, 2035–2043.

Battjes, J.A., Groenendijk, H.W., 2000. Wave height distributions on shallow foreshores. Coast. Eng. 40, 161–182.

Bowen, A.J., 1980. Simple models for nearshore sedimentation: beach profiles and longshore bars. Coastline of Canada, Geol. Surv. Canada, pp. 1–11.

Cornish, V., 1898. On sea beaches and sand banks. Geol. 2, 628–674.

Doering, J.C., Bowen, A.J., 1995. Parameterization of orbital velocity asymmetries of shoaling and breaking waves using bispectral analysis. Coast. Eng. 26, 15–33.

Doering, John C., Elfrink, B., Hanes, Daniel M., Ruessink, B.G., 2000. Parameterization of velocity skewness. Proceedings 27th Int. Conference on Coastal Engineering, ASCE, Sydney, Australia, 16–20 July 2000, pp. 1383–1396.

Elfrink, B., Rakha, K.A., Deigaard, R., Brøker, I., 1999. Effect of near-bed Velocity Skewness on Cross Shore Sediment Transport. Proc. Coastal Sediments '99, Long Island, NY, pp. 33–47.

Elgar, S.L., Guza, R.T., 1986. Nonlinear model predictions of shoaling surface gravity waves. J. Fluid Mech. 167, 1–18.

Elgar, S.L., Freilich, M.H., Guza, R.T., 1990. Model-data comparisons of moments of nonbreaking shoaling surface gravity waves. J. Geophys. Res. 95 (C9), 16,055–16,063.

Forsythe, G.E., 1957. Generation and use of orthogonal polynomials for datafitting with a digital computer. J. Siam Soc. 5, 74–88.

Grasmeijer, B.T., Van Rijn, L.C., 1998. Breaker bar formation and migration. Proc. 26th International Conference on Coastal Engineering. ICCE'98, Copenhagen, Denmark. ASCE, pp. 2750–2758.

Hamm, L., 1996. Computation of the near-bottom kinematics of shoaling waves. Proc. 25th International Conference on Coastal Engineering. ICCE'96. Orlando, USA. ASCE, pp. 537–550.

Hamm, L., Peronnard, C., 1997. Wave parameters in the nearshore: a clarification. Coast. Eng. 32, 119–135.

Hanes, D.M., Jette, C.D., Thosteson, E.D., Vincent, C.E., 1998. Field observations of nearshore, wave–seabed interactions. Coastal Dynamics '97, ASCE, 11–18. Plymouth, U.K. , pp. 23–37.

Hanes, D.M., Alymov, V., Chang, Y.S., 2001. Wave formed sand ripples at Duck, North Carolina. J. Geophys. Res. — Oceans 106 (C10), 22575–22592.

Inman, D.L., Bagnold, R.A., 1963. Littoral Processes. Sea 3, 529–543.

Isobe, M., Horikawa, K., 1982. Study on water particle velocities of shoaling and breaking waves. Coast. Eng. Jpn. 25, 109–123.

Keijzer, M., Babovic, V., 1999. Dimensionally aware genetic programming. Proc. of the Genetic and Evolutionary Algorithm Conf., July 13 – 17, 1999, Orlando, FL, pp. 1069–1076.

Kennedy, A.B., Chen, Q., Kirby, J.T., Dalrymple, R.A., 2000. Boussinesq modeling of wave transformation, breaking and runup1: 1D. J. Waterw. Port Coast. Ocean Eng. 126 (1), 39–47.

Klopman, G., 1996. Extreme wave heights in shallow water, Report H2486, WL/Delft Hydraulics, The Netherlands.

Madsen, P.A., Sørensen, O.R., Schäffer, H.A., 1997. Surf zone dynamics simulated by a Boussinesq type model. Part 2: surf beat and swash oscillations for wave groups and irregular waves. Coast. Eng. 32, 289–319.

Ruessink, B.G., Houwman, K.T., Hoekstra, P., 1998. The systematic contribution of transporting mechanisms to the cross-shore sediment transport in water depths of 3 to 9 m. Mar. Geol. 152, 295–324.

Ruessink, B.G., van Enckevort, I.M.J., Kingston, K.S., Davidson, M.A., 2000. Observations of two- and three-dimensional sandbar behaviour. Mar. Geol. 169, 161–183.

Stokes, G.G., 1847. On the theory of oscillatory waves. Trans. Camb. Philos. Soc. 8, 441–455.

Swart, D.H., Loubster, C.C., 1978. Vocoidal water wave theory for all non-breaking waves. Proc. 16th Int. Conference on Coastal Engineering (ICCE). ASCE, Hamburg, Germany, pp. 467–486.

Veeramony, J., Svendsen, I.A., 2000. The flow in surf zone waves. Coast. Eng. 39, 93–122.

Wells, D.R., 1967. Beach equilibrium and second-order wave theory. J. Geophys. Res. 72, 497–504.